AIAA SciTech
13-17 January 2014, National Harbor, Maryland
AIAA Guidance, Navigation, and Control Conference

Adaptive Control of a Flapping Wing Robot Inspired by Bat Flight

Shirin Dadashi, Jessica Gregory, Yu Lei , Matt Bender
Virginia Tech, Blacksburg, Virginia, USA
Andrew Kurdila*, Javid Bayandor†, Rolf Müller‡

Downloaded by UNIV OF CALIFORNIA LOS ANGELES on May 2, 2014 | http://arc.aiaa.org | DOI: 10.2514/6.2014-0086

This paper describes the formulation of the equations of kinematics for a flapping wing robot inspired by observations of bats in flight, the derivation of the governing equations of motion for the robot, and the construction of an adaptive controller to track the observed flapping motion. The kinematics of the articulated flapping wings is represented using the Denavit-Hartenberg convention to facilitate a compact and simple description of the degrees of freedom of the robot that can be used by biologists to summarize assumptions on bat motion. The equations of motion of the bat robotic system are derived using Lagrange's equations in which the virtual work of the pressure forces on the wings is calculated by assuming a quasi-steady approximation of the aerodynamic forces. The derived controller guarantees asymptotic convergence of the tracking error and derivative of the tracking error. Additionally, the convergence of estimates of the lift and drag acting on each wing section is established whenever standard persistency of excitation conditions hold.

I. Introduction

The analysis, design, fabrication and experimental testing of flapping wing robots has experienced a renaissance of sorts over the past several years. This trend has been well-documented in research that investigates the aerodynamics, flight mechanics, and control of micro-air-vehicles (MAVs) in, for example, [24] and [33]. Studies to understand the aerodynamics of flapping flight have appeared to enable design of flapping wing vehicles. These efforts include studies of insects, birds and bats in [5, 7–9, 13, 16, 17, 35]. While the motion of flapping wings in certain insects can be described with relatively few parameters, the flapping motions of birds and bats are achieved via complex, articulated wings. The beat frequency, amplitude, and phasing among the various parts of the wings vary among flight regimes for a specific bird or bat, and also vary across species. Structural parameters such as camber, chord, wing area, and wing length also affect the lift and drag generated by the articulated wings. Impressive progress in measuring flapping motions in flight using digital imaging systems has been reported in [5, 8], for example. However, the experimental assessment of lift and drag generated by articulated flapping wings remains extremely difficult. While some insect studies have mounted specimens to load measuring devices for evaluation of aerodynamic loads, this approach is not feasible for bats or birds. Because of the complexity, difficulty and cost of making measurements of flapping articulated wings during flight, there have appeared several efforts to design, build, and control robots that emulate flapping flight regimes in the laboratory or in a wind tunnel. If the motion of flapping wings observed in nature can be replicated, or at least closely approximated, the assessment of aerodynamic performance for complex articulated flapping motions can be carried out via laboratory or wind tunnel study of flapping wing robots. Of particular interest to this paper are the efforts in [6] and [2] that describe the design and fabrication of robots to study the flapping motion and aerodynamics of bats.

This paper extends the work of the authors in [1, 3] that treats the control of robots to track flapping flight motions observed in birds. In this paper we derive the equations of motion and an adaptive control strategy to track flapping wing motions observed in bats based on the simplified robotic system described in [2]. The kinematics of the robot are defined using the Denavit-Hartenberg convention [15] so as to provide a simple, compact description of the kinematics

*Center for Dynamic Systems and Modeling (DySMAC), Department of Mechanical Engineering, Virginia Tech
†Crashworthiness for Aerospace Structures and Hybrids (CRASH) Lab, Department of Mechanical Engineering, Virginia Tech, AIAA Associate Fellow
‡Department of Mechanical Engineering, Virginia Tech and Shandong University - Virginia Tech International Laboratory

Copyright © 2014 by the American Institute of Aeronautics and Astronautics, Inc. All rights reserved.

that can be easily summarized and communicated by biologists in the academic community. The equations of motion are derived for the flapping wing robot using Lagrange's equations where the contributions of the aerodynamics to the virtual work are calculated using a quasi-steady model of the aerodynamics. The resulting equations are subsequently written in "linear-in-parameters" first order form, a mathematical structure that has been studied systematically in the community of researchers studying control of robotic systems. An adaptive controller is derived that guarantees that the robot will track asymptotically the joint angles and joint angle rates of bats observed in flight. Additionally, the derived controller will generate online estimates of the lift and drag generated by the flapping motion, provided certain standard conditions on persistency of excitation hold.

II. Denavit-Hartenberg Convention for the Robotic Bat

Careful study of the morphology of bats suggests that a detailed multibody dynamics model of their bioskeletal structure would include 34 degrees of freedom to represent wing kinematics [2]. Such a high dimensional model is not likely to be feasible for use in a real-time feedback control strategy, and the cost of instrumenting such a complex robotic system to make simultaneous measurements of all the degrees of freedom would likewise be prohibitive. A model of reduced complexity, one that captures the essential features of the observed flapping motion is required. The approach that follows is based on the robotic bat design described in [2], but it will be clear from the discussion that the general strategy is applicable in general. We use the Denavit-Hartenberg convention to construct a model of the bat wing. The joint between link i and $i+1$ is labelled joint i and to each joint we associate the joint angle θ_i. Each angle θ_i rotates about axis $\mathbf{z}_{i-1}$ from $\mathbf{x}_{i-1}$ to $\mathbf{x}_i$. Below is a schematic of the robotic wing proposed in [2]. Each axis of rotation is shown attached to links of the wing. We have attached the axes of rotation to the link that rotates about them. This has the effect of putting an axis of rotation $\mathbf{z}_i$ which is actually grounded to link i on link $i+1$. We do this because we are interested in how link $i+1$ rotates relative to link i. Link 1 is not labelled because it is a massless link associated with the shoulder. Inside the shoulder piece is a gimbal with two degrees of freedom. We represent the rotations by assigning θ_1, with axis of rotation z_0 as one, and θ_2, with axis of rotation z_1 as the other.

Having established the axes of rotation we can now construct the i^{th} frames for link i. Recall that the Denavit-Hartenberg convention requires that x_i be perpendicular and intersect $\mathbf{z}_{i-1}$. We begin with link 0 by arbitrarily assigning $\mathbf{x}_0$ and $\mathbf{y}_0$ and then construct the frame for link 1. All of our frame vectors are unit vectors. We compile our results in the following table where θ_i represents the angle between $\mathbf{x}_{i-1}$ and $\mathbf{x}_i$, α_i represents the angle between $\mathbf{z}_{i-1}$ and $\mathbf{z}_i$, d_i represents the perpendicular distance between $\mathbf{x}_{i-1}$ and $\mathbf{x}_i$, and a_i represents the perpendicular distance between $\mathbf{z}_{i-1}$ and $\mathbf{z}_i$.

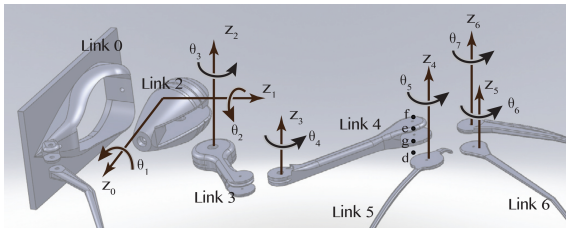

Figure 1. ROBOTIC BAT, DEGREES OF FREEDOM, AND DOF AXES- Adopted from [2] page 5 Figure 3

Table 1 completely summarizes the kinematic representation. It provides a compact and succinct means for biologists to convey their underlying assumptions regarding the motion observed in nature. For example, this table shows that there are only 7 physical parameters that dictate the specific flapping motions that are possible to represent with this 7 degree of freedom model.

Link i	θ_i	α_i	d_i	a_i
Link 1	$\theta_1(t)$	$\frac{\pi}{2}$	0	0
Link 2	$\theta_2(t)$	$\frac{\pi}{2}$	$d_{a,h}$	$d_{b,h}$
Link 3	$\theta_3(t)$	0	0	$d_{b,c}$
Link 4	$\theta_4(t)$	0	0	$d_{c,g}$
Link 5	$\theta_5(t)$	0	$-d_{g,d}$	0
Link 6	$\theta_6(t)$	0	$d_{d,e}$	0
Link 7	$\theta_7(t)$	0	$d_{e,f}$	0

Downloaded by UNIV OF CALIFORNIA LOS ANGELES on May 2, 2014 | http://arc.aiaa.org | DOI: 10.2514/6.2014-0086

Table 1. DH Parameters

In fact, as we show more fully in our numerical experiments, further simplification is possible in many cases. If (a) the origins of frames $0,1,2$ coincide at the shoulder center and (b) the origins of the frames $4,5,6,7$ are taken as the wrist center, then there are only two parameters that vary in this flight model across species. As a final step in describing the kinematics, we orient each frame i within link i. Above we established the relationship between the frames of link $i-1$ and link i without concern of how the axes align with the rigid components of the wing. In the figure below we have superimposed our orientation of each frame i onto the schematic of the wing.

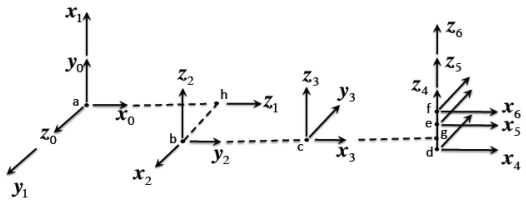

Figure 2. Schematic of Frame Definitions and Parameters

III. Inverse Kinematics Problem

DH parameters are one of the common choices used to represent robotic systems that have the form of kinematic chains, or of systems having the connectivity of a topological tree. In this section we describe the solution of the inverse kinematics problem wherein observations of flight motions is used to generate trajectories suitable for tracking control. We suppose that we are provided with inertial trajectories of *feature points* fixed on the wings of bats in flight. These trajectories are typically the output of structure from motion (SFM) or simultaneous localization and mapping algorithms (SLAM) applied to sequences of frames obtained from monocular or stereo cameras used to image bats in flight. See [5, 8] for example experimental studies. From table 1 we can determine the kinematics of any of these feature points on the wing via the relation,

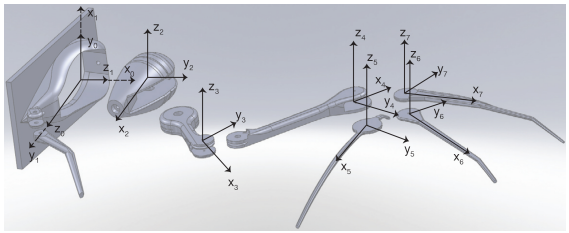

Figure 3. BODY FIXED FRAMES- Adopted from [2] page 5 Figure 3

$$\mathbf{p}^0_{k,j} = \mathbf{H}^0_k(\theta_1(t),\theta_2(t),\ldots,\theta_k(t))\mathbf{p}^k_{k,j} \tag{1}$$

where $j = 1,\ldots,n_k$ represents the j^{th} feature point on the k^{th} body, $\mathbf{p}^0_{k,j}$ is the vector of homogeneous coordinates for this feature point in terms of the 0^{th} frame, and $\mathbf{p}^k_{k,j}$ is the vector of homogeneous coordinates for the j^{th} feature point in terms of frame k. Writing equation 1 explicit form we have,

$$\mathbf{p}^0_{k,j} = \mathbf{H}^0_1(\theta_1(t))\mathbf{H}^1_2(\theta_2(t))\cdots\mathbf{H}^{k-1}_k(\theta_k(t))\mathbf{p}^k_{k,j} \tag{2}$$

The homogeneous transforms $\mathbf{H}^{i-1}_i$ that relates the coordinates in frame i to those in frame $i-1$ are easily computed from table 1 [15]. The accuracy of any set of joint variables $\left\{\theta_1(t)\cdots\theta_N(t)\right\}$ substituted into equation 2 can be assessed by the norm of the error

$$\left\|\hat{\mathbf{p}}^0_{k,j}(t) - \mathbf{p}^0_{k,j}(t)\right\| \tag{3}$$

where $\hat{\mathbf{p}}^0_{k,j}(t)$ is the experimental value of the location at time t of the feature point j on body k. Experimental data is sampled by nature, and the discrete form of an optimization problem for the joint angles $\left\{\theta_1(t)\cdots\theta_N(t)\right\}$ can be cast in terms of an error functional written as

$$\mathcal{J}(t,\theta_1(t),\ldots,\theta_N(t)) = \sum_{k=1}^{N}\sum_{j=1}^{n_k} w_{tkj}\left\|\hat{\mathbf{p}}^0_{k,j}(t) - \prod_{1,\ldots,k}\mathbf{H}^0_1(\theta_1(t))\cdots\mathbf{H}^{k-1}_k(\theta_k(t))\mathbf{p}^k_{j,k}\right\|^2 \tag{4}$$

Downloaded by UNIV OF CALIFORNIA LOS ANGELES on May 2, 2014 | http://arc.aiaa.org | DOI: 10.2514/6.2014-0086

where we sum over the links $k = 1, \ldots, N$ and the feature points j. The constants w_{kj} are positive constants that weight the relative importance of various feature points. Many different types of reasonable optimization problems can be cast in terms of the functional $\mathcal{J}$. At each time t_m at which experimental data is available, we can seek to solve for the joint angles $\left\{\theta_1^*(t_m) \cdots \theta_N^*(t_m)\right\}$ such that

$$\left\{\theta_1^*(t_m) \cdots \theta_N^*(t_m)\right\} = \underset{\left\{\theta_1(t_m) \ldots \theta_N(t_m)\right\} \in \boldsymbol{\Theta}}{\text{arginf}} \quad \mathcal{J}(t_m, \theta_1(t_m), \ldots, \theta_N(t_m))$$

where $\boldsymbol{\Theta} \subseteq \mathbb{R}^N$ is the set of admissible joint angles. This formulation has the advantage that each optimization problem at time t_m is small, having N unknowns, and is decoupled from the rest. Since the experimental observations are noisy, however, the trajectory of identified joint angles $\left\{\theta_1(t_m) \cdots \theta_N(t_m)\right\}_{m \in \mathbb{N}}$ can be nonsmooth. Alternatively, it is possible to represent the unknown trajectory of joint angles in terms of smoothing splines

$$\theta_1(t, \boldsymbol{\alpha}_1) := \sum_n \psi_n(t) \alpha_{1,n}$$

$$\vdots$$

$$\theta_N(t, \boldsymbol{\alpha}_N) := \sum_n \psi_n(t) \alpha_{N,n}$$

where $\alpha_{i,n}$ is the n^{th} knot of the spline used to represent the angle $\theta_i(t)$, the vector $\boldsymbol{\alpha}_i := \left\{\alpha_{i,1} \ldots \alpha_{i,M}\right\}$, and M is the number of spline functions. We seek the knot sequences $\left\{\boldsymbol{\alpha}_1^* \ldots \boldsymbol{\alpha}_N^*\right\}$ such that

$$\left\{\boldsymbol{\alpha}_1^* \ldots \boldsymbol{\alpha}_N^*\right\} = \underset{\left\{\boldsymbol{\alpha}_1 \ldots \boldsymbol{\alpha}_N\right\} \in \mathcal{A}_1 \times \cdots \times \mathcal{A}_N}{\text{arginf}} \quad \sum_{m \in \mathbb{N}} w_m \mathcal{J}(t_m, \theta_1(t_m, \boldsymbol{\alpha}_1), \ldots, \theta_N(t_m, \boldsymbol{\alpha}_N))$$

where w_m is a positive constant that weights the importance of each time step and $\mathcal{A}_1 \times \cdots \mathcal{A}_N$ is the set of permissible knot sequences. This optimization problem yields smoother trajectories of estimated joint angles, but is more computationally costly. The optimization problem is expressed in terms of $N \times M$ unknowns.

IV. Equations of Robotics

The equations of motion of the flapping wing robot can be written using Lagrange's equations. We define the kinetic energy $T = T(\mathbf{q}(t), \dot{\mathbf{q}}(t), t)$ and the potential energy $V = V(\mathbf{q}(t))$ of the system (the bat wing) in terms of the generalized coordinates $\mathbf{q}(t)$ and $\dot{\mathbf{q}}(t)$. The generalized coordinates for the bat wing are $\mathbf{q}(t) = \begin{bmatrix}\theta_1(t) & \cdots & \theta_7(t)\end{bmatrix}^{\mathrm{T}}$ and $\dot{\mathbf{q}}(t) = \begin{bmatrix}\dot{\theta}_1(t) & \cdots & \dot{\theta}_7(t)\end{bmatrix}^{\mathrm{T}}$. An explicit form for the kinetic energy can be written in terms of the summation over the links

$$T = \frac{1}{2} \sum_{k=1}^{N} m_k \mathbf{v}_{0,c_k}^{\mathrm{T}} \cdot \mathbf{v}_{0,c_k} + \frac{1}{2} \sum_{k=1}^{N} \boldsymbol{\omega}_{0,k}^{\mathrm{T}} \mathbf{I}_k \boldsymbol{\omega}_{0,k} \tag{5}$$

The term $\mathbf{I}_k$ is the inertia matrix with respect to a frame that has its origin at the center of mass of link k and is parallel to the k^{th} frame. The 3-tuples $\mathbf{v}_{0,c_k}^0$ and $\boldsymbol{\omega}_{0,k}^0$ are the components of the velocities $\boldsymbol{v}_{0,k}$ and angular velocities $\boldsymbol{\omega}_{0,k}$, respectively, relative to the basis for the inertial frame. They are calculated from the generalized coordinate $\dot{\mathbf{q}}(t)$ and the $3 \times k$ Jacobian matrices [15] $\mathbf{J}_{v_k}^0, \mathbf{J}_{\omega_k}^0$ as below,

$$\begin{bmatrix}\mathbf{v}_{0,c_k}^0 \\ \boldsymbol{\omega}_{0,k}^0\end{bmatrix} = \begin{bmatrix}\mathbf{J}_{\mathbf{v}_k}^0 \\ \mathbf{J}_{\boldsymbol{\omega}_k}^0\end{bmatrix} \dot{\mathbf{q}} \tag{6}$$

The kinetic energy is obtained by substituting equation 6 into equation 5 to get

$$T = \frac{1}{2} \dot{\mathbf{q}}^{\mathrm{T}} \underbrace{\left(\sum_k m_k \mathbf{J}_{v_k}^{0,\mathrm{T}} \mathbf{J}_{v_k}^0 \right)}_{\mathbf{M}_{\mathbf{v}}} \dot{\mathbf{q}} + \frac{1}{2} \dot{\mathbf{q}}^{\mathrm{T}} \underbrace{\left(\sum_k \mathbf{J}_{\omega_k}^{0,\mathrm{T}} \mathbf{I}_k^0 \mathbf{J}_{\omega_k}^0 \right)}_{\mathbf{M}_{\boldsymbol{\omega}}} \dot{\mathbf{q}} \tag{7}$$

Downloaded by UNIV OF CALIFORNIA LOS ANGELES on May 2, 2014 | http://arc.aiaa.org | DOI: 10.2514/6.2014-0086

To formulate the equation of motions, we use Lagrange's equation which hold that for each $k = 1, \ldots, N$ that

$$\frac{d}{dt}\left(\frac{\partial T}{\partial \dot{q}_k}\right) - \frac{\partial T}{\partial q_k} + \frac{\partial V}{\partial q_k} = Q_k$$

The generalized forces Q_k are obtained by calculating the total virtual work

$$\delta W = \sum_k \mathbf{F}_{0,p_k} \cdot \delta \mathbf{r}_{0,cp_k} = \sum_k Q_k \, \delta q_k$$

The equations derived as above from Lagrange's equation are written as the following set of coupled, nonlinear second order ordinary differential equations

$$\mathbf{M}(\mathbf{q})\ddot{\mathbf{q}}(t) = \mathbf{n}(\mathbf{q}(t), \dot{\mathbf{q}}(t)) + \mathbf{B}(\mathbf{q}(t))\mathbf{u}(t)$$

where $\mathbf{M} = \mathbf{M}_\mathbf{v} + \mathbf{M}_\omega$ is the generalized mass/inertia matrix, $\mathbf{n}(\cdot, \cdot)$ is the non-linear right-hand side including centripetal and Coriolis terms, $\mathbf{B}(\cdot)$ the control influence matrix and $\mathbf{u}(\cdot)$ contains input actuation forces and torques.

Downloaded by UNIV OF CALIFORNIA LOS ANGELES on May 2, 2014 | http://arc.aiaa.org | DOI: 10.2514/6.2014-0086

V. Control Formulation and Numerical Results

The control of robotic systems whose governing equations have the form in Equation IV has been studied systematically. See [15, 29, 32] for an overview. The control of flapping wing robots, however, pose significant additional difficulties beyond those of conventional robotic systems. Most importantly, the aerodynamic contributions to the equations of motion for flapping wing robots must have a magnitude that is commensurate with that of the inertial terms. These aerodynamic terms are unknown and cannot be measured in real time, for reasons summarized in the introduction. In this section we describe the formulation of an adaptive control scheme that will generate motions that track those observed in nature. The control objective is to design the adaptive controller so that the output signal, $\mathbf{y}(t)$, tracks the desired trajectory, $\mathbf{r}(t)$. We design a self-organizing adaptive controller.

A few preliminary steps are required to put the equations of motion in a form suitable for control synthesis. The nonlinear right hand side vector $\mathbf{n}$ is decomposed into geometric contributions $\mathbf{n}_g$ due the centripetal and Coriolis terms and $\mathbf{n}_a$ due to the aerodynamic loads.

$$\mathbf{n}(\mathbf{q}(t), \dot{\mathbf{q}}(t)) := \mathbf{n}_g(\mathbf{q}(t), \dot{\mathbf{q}}(t)) + \mathbf{n}_a(\mathbf{q}(t), \dot{\mathbf{q}}(t)) \tag{8}$$

The formulation of the control problem first casts the equations in first order form. We solve the second order form of the governing equations for the second derivatives,

$$\ddot{\mathbf{q}}(t) = \mathbf{M}^{-1}(\mathbf{q}(t))\mathbf{n}_g(\mathbf{q}(t), \dot{\mathbf{q}}(t)) + \mathbf{M}^{-1}(\mathbf{q}(t))(\boldsymbol{u}(t) + \mathbf{n}_a(\mathbf{q}(t), \dot{\mathbf{q}}(t)) \tag{9}$$

We introduce the state space variables $\mathbf{X}(t) := \left[\mathbf{X}_1(t)^T \; \mathbf{X}_2(t)^T\right]^T = \left[\mathbf{q}(t)^T \; \dot{\mathbf{q}}(t)^T\right]^T$ and choose the feedback linearizing control law $\boldsymbol{u}(t) = \mathbf{M}(\mathbf{X}_1(t))(\boldsymbol{G}_1\mathbf{X}_1(t) + \boldsymbol{G}_2\mathbf{X}_2(t)) + \mathbf{n}_g(\mathbf{X}_1(t), \mathbf{X}_2(t)) - \boldsymbol{v}(t)$. The system dynamics can be written as

$$\begin{aligned}\dot{\mathbf{X}}(t) &= \begin{bmatrix}\dot{\mathbf{X}}_1(t) \\ \dot{\mathbf{X}}_2(t)\end{bmatrix} = \begin{bmatrix}0_n & \boldsymbol{I}_n \\ \boldsymbol{G}_1 & \boldsymbol{G}_2\end{bmatrix}\begin{bmatrix}\mathbf{X}_1(t) \\ \mathbf{X}_2(t)\end{bmatrix} + \begin{bmatrix}0 \\ \mathbf{M}^{-1}(\mathbf{X}_1(t))(\mathbf{n}_a - \boldsymbol{v}(t))\end{bmatrix} \\ &= \mathbf{A}_m\mathbf{X}(t) + \mathbf{B}(\mathbf{f}(\mathbf{X}(t)) - \boldsymbol{v}(t))\end{aligned} \tag{10}$$

We choose the gain matrices $\boldsymbol{G}_1$ and $\boldsymbol{G}_2$ matrices so that the matrix $\mathbf{A}_m$ is Hurwitz. The synthesis of an L^1 controller requires that we introduce the state predictor equation

$$\dot{\hat{\mathbf{X}}}(t) = \mathbf{A}_m\hat{\mathbf{X}}(t) + \mathbf{B}(\hat{\mathbf{f}}(\mathbf{X}(t) - \boldsymbol{v}(t)). \tag{11}$$

Our goal is to construct an adaptive approximation to the unknown function $\mathbf{f}(\mathbf{X}(t))$ such that the error between the predicted state and the actual state tends to zero or remains bounded. As a result, $\hat{\mathbf{f}}(\mathbf{X}(t))$ will estimate the real aerodynamic function $\mathbf{f}(\mathbf{X}(t))$ with a bounded approximation error. The intent is to cancel out the unknown aerodynamic contribution via generating the input function equal to $\hat{\mathbf{f}}(\mathbf{X}(t))$. In [3], it is shown that the contribution of the

aerodynamic forces to the equations of motion can be written in terms of the matrix $\mathbf{\Psi}$,

$$\mathbf{\Psi} = -\left[\left(\mathbf{J}^{B_1}_{\mathbf{v}_{a_1}}\right)^{\mathrm{T}}\left(\mathbf{R}^{S_1}_{B_1}\right)^{\mathrm{T}} \quad \dots \quad \left(\mathbf{J}^{B_N}_{\mathbf{v}_{a_N}}\right)^{\mathrm{T}}\left(\mathbf{R}^{S_N}_{B_N}\right)^{\mathrm{T}}\right]\left[\mathrm{diag}\begin{bmatrix}1 & 0\\ 0 & 0\\ 0 & 1\end{bmatrix}\right]$$

via the equation

$$\mathbf{n}_a = \mathbf{\Psi}\begin{Bmatrix} D_1 \\ L_1 \\ \vdots \\ D_N \\ L_N \end{Bmatrix}$$

where $\boldsymbol{J}^{\boldsymbol{B}_k}_{\boldsymbol{v}_{a_k}}$ is the Jacobian matrix associated with the velocity of the aerodynamic center of link k, $\mathbf{R}^{S_k}_{\boldsymbol{B}_k}$ is the rotation matrix that maps the body fixed frame $\boldsymbol{B}_k$ into the frame S_k for the stability axes of the frame k, $D_1,\dots,D_N$ are the drag forces acting on wing sections $1,\dots,N$, and $L_1,\dots,L_N$ are the lift forces acting on the wing sections $1,\dots,N$.

The crucial step in the synthesis of the controller in this paper is to build an observer dynamics for the aerodynamic contributions to the model. Since the state equations have been transformed into the following form that depends on the new control input $\boldsymbol{\nu}(t)$,

$$\dot{\mathbf{X}}(t) = \mathbf{A}_m\mathbf{X}(t) + \mathbf{B}\begin{bmatrix} 0_n \\ \mathbf{n}_a(\mathbf{X}(t)) - \boldsymbol{\nu}(t)\end{bmatrix},$$

the observer dynamics is governed by the equation

$$\dot{\hat{\mathbf{X}}}(t) = \mathbf{A}_m\hat{\mathbf{X}}(t) + \mathbf{B}\begin{bmatrix} \mathbf{0} \\ \hat{\mathbf{n}}_a(\mathbf{X}(t)) - \boldsymbol{\nu}(t)\end{bmatrix}$$

Here the function $\mathbf{B}$ is in fact the matrix $\mathbf{M}^{-1}(\mathbf{X}_1(t))$. Therefore, the the tracking error $\tilde{\mathbf{X}} := \mathbf{X} - \hat{\mathbf{X}}$ satisfies the equation

$$\dot{\tilde{\mathbf{X}}}(t) = \mathbf{A}_m\tilde{\mathbf{X}}(t) + \mathbf{B}\begin{bmatrix} \mathbf{0} \\ \hat{\mathbf{n}}_a(\mathbf{X}(t)) - \mathbf{n}_a(\mathbf{X}(t))\end{bmatrix}$$

The assumption that $\mathbf{n}_a$ are generated by a quasi steady aerodynamic model as discussed in [3] implies that the final model depends linearly on the unknown parameters that describe the lift and the drag forces on each wing. We can organize the aerodynamic contributions to the equations of motion $\mathbf{n}_a$ and their estimates $\hat{\mathbf{n}}_a$ as

$$\begin{bmatrix} \hat{\mathbf{n}}_{a,1} - \mathbf{n}_{a,1} \\ \vdots \\ \hat{\mathbf{n}}_{a,N} - \mathbf{n}_{a,N}\end{bmatrix} = \mathbf{\Psi}(\mathbf{X})\begin{bmatrix} \hat{D}_1(\alpha_1(\mathbf{X})) - D_1(\alpha_1(\mathbf{X})) \\ \hat{L}_1(\alpha_1(\mathbf{X})) - L_1(\alpha_1(\mathbf{X})) \\ \vdots \\ \hat{D}_N(\alpha_1(\mathbf{X})) - D_N(\alpha_n(\mathbf{X})) \\ \hat{L}_N(\alpha_1(\mathbf{X})) - L_N(\alpha_n(\mathbf{X}))\end{bmatrix}$$

When we define the block diagonal matrix Ξ as

$$\Xi = \mathbf{\Psi}(\mathbf{X})\begin{bmatrix} \frac{1}{2}\rho\begin{bmatrix}\Delta V_1^2 A_1 & 0 \\ 0 & \Delta V_1^2 A_1\end{bmatrix} & & \\ & \ddots & \\ & & \frac{1}{2}\rho\begin{bmatrix}\Delta V_N^2 A_N & 0 \\ 0 & \Delta V_N^2 A_N\end{bmatrix}\end{bmatrix}$$

where $\Delta V_i^2 := \|\boldsymbol{\nu}_{0,a_i} - \boldsymbol{\nu}_{0,w}\|^2$ is equal to the square of the norm of the difference of the velocity of the aerodynamic center $\boldsymbol{\nu}_{0,a_i}$ of wing section i and the wind velocity $\boldsymbol{\nu}_{0,w}$, A_i is the wing area of the i^{th} wing section, and ρ is the density of air.

$$\begin{bmatrix} \hat{\mathbf{n}}_{a,1} - \mathbf{n}_{a,1} \\ \vdots \\ \hat{\mathbf{n}}_{a,N} - \mathbf{n}_{a,N}\end{bmatrix} = \Xi(\mathbf{X})\begin{bmatrix} \hat{c}_{d,1}(\alpha_1(\mathbf{X})) - c_{d,1}(\alpha_1(\mathbf{X})) \\ \hat{c}_{l,1}(\alpha_1(\mathbf{X})) - c_{l,1}(\alpha_1(\mathbf{X})) \\ \vdots \\ \hat{c}_{d,N}(\alpha_n(\mathbf{X})) - c_{d,N}(\alpha_N(\mathbf{X})) \\ \hat{c}_{l,N}(\alpha_n(\mathbf{X})) - c_{l,N}(\alpha_N(\mathbf{X}))\end{bmatrix}$$

Downloaded by UNIV OF CALIFORNIA LOS ANGELES on May 2, 2014 | http://arc.aiaa.org | DOI: 10.2514/6.2014-0086

The lift L_i and drag forces D_i on wing section i, and their estimates $\hat{L}_i$ and $\hat{D}_i$, respectively, are estimated in terms of the lift and drag coefficients $c_{l,i}$ and $c_{d,i}$, and their estimates $\hat{c}_{l,i}$ and $\hat{c}_{d,i}$ in the form

$$\hat{c}_{d,i}(\alpha_i) - c_{d,i}(\alpha_i) = \boldsymbol{\phi}_i^T(\alpha_i)(\hat{\boldsymbol{w}}_{d,i} - \boldsymbol{w}_{d,i}^*) = \phi_i^T(\alpha_i)\tilde{\boldsymbol{w}}_{d,i}$$

$$\hat{c}_{l,i}(\alpha_i) - c_{l,i}(\alpha_i) = \boldsymbol{\phi}_i^T(\alpha_i)(\hat{\boldsymbol{w}}_{l,i} - \boldsymbol{w}_{l,i}^*) = \phi_n^T(\alpha_{l,i})\tilde{\boldsymbol{w}}_{l,i}$$

where the approximations are given as

$$\dot{\tilde{\mathbf{X}}} = \mathbf{A}_m\tilde{\mathbf{X}} + \begin{bmatrix} \mathbf{0} \\ \mathbf{M}^{-1}(\mathbf{X}_1)\Xi \begin{bmatrix} \boldsymbol{\phi}_1^T(\alpha_1)\mathbb{I}_2 & & \\ & \ddots & \\ & & \boldsymbol{\phi}_N^T(\alpha_N)\mathbb{I}_2 \end{bmatrix} \begin{bmatrix} \tilde{w}_{d,1} \\ \tilde{w}_{l,1} \\ \vdots \\ \tilde{w}_{d,N} \\ \tilde{w}_{l,N} \end{bmatrix} \end{bmatrix}$$

The vectors $\boldsymbol{\phi}_i(\alpha_i) := \left\{\phi_1(\alpha_i)\ldots\phi_{N_i}(\alpha_i)\right\}$ contain the basis functions used to approximate the lift and drag on wing section i. We introduce the matrix $\boldsymbol{\Phi}^T$ in the equation

$$\boldsymbol{\Phi}^T = \begin{bmatrix} \boldsymbol{\phi}_1^T(\alpha_1)\mathbb{I}_2 & & \\ & \ddots & \\ & & \boldsymbol{\phi}_n^T(\alpha_n)\mathbb{I}_2 \end{bmatrix}$$

and stack the unknown parameter errors in the vector $\tilde{\boldsymbol{W}}$

$$\tilde{\boldsymbol{W}} = \begin{bmatrix} \tilde{\boldsymbol{w}}_{d,1} \\ \tilde{\boldsymbol{w}}_{l1} \\ \vdots \\ \tilde{\boldsymbol{w}}_{d,N} \\ \tilde{\boldsymbol{w}}_{l,N} \end{bmatrix}$$

to obtain the final, linear-in-parameters equation the governs the tracking error

$$\dot{\tilde{\mathbf{X}}} = \mathbf{A}_m\tilde{\mathbf{X}} + \mathcal{B}\boldsymbol{\Phi}^T(\alpha_1, \cdots, \alpha_N)\tilde{\boldsymbol{W}}$$

This equation contains the modified control influence operator $\mathcal{B}$

$$\mathcal{B} = \begin{bmatrix} \mathbf{0} \\ \mathbb{I} \end{bmatrix} \mathbf{M}^{-1}\Xi$$

The adaptive control strategy is defined in terms of the the Lyapunov function

$$V = \tilde{\mathbf{X}}^T\mathbf{P}\tilde{\mathbf{X}} + \tilde{\boldsymbol{W}}^T\tilde{\boldsymbol{W}}$$

and the learning law for the unknown parameters given in the equation

$$\dot{\tilde{\boldsymbol{W}}} = -\boldsymbol{\Phi}\mathcal{B}^T\boldsymbol{P}\tilde{\mathbf{X}}$$

The Locally Weighted Learning (LWL) technique has been exploited to approximate the drag/lift function [39] which are shown here as $C_{DL}(\alpha)$ for each wing section. As mentioned before, the vector drag/lift profile is formed by $\hat{C}_{DL} = \boldsymbol{\Phi}^T(\alpha)\hat{\boldsymbol{W}}$.Then the approximation to $C_{DL}(\alpha)$ at point α is written in the form of normalized weighted average of local approximators $\hat{C}_{DL,k}$,

$$\hat{C}_{DL}(\alpha) = \frac{\sum_k \omega_k(\alpha)\hat{C}_{DL,k}(\alpha)}{\sum_k \omega_k(\alpha)}.$$

In which

$$\omega_k(\alpha) = \begin{cases} (1 - (\frac{\|\alpha - c_k\|}{\mu})^2)^2 & \text{for } \|\alpha - c_k\| < \mu \\ 0 & \text{otherwise.} \end{cases}$$

Downloaded by UNIV OF CALIFORNIA LOS ANGELES on May 2, 2014 | http://arc.aiaa.org | DOI: 10.2514/6.2014-0086

where $c_k \in \mathbb{R}$ is the center location of the $k-$th weighting function. $\mu \in \mathbb{R}$ represents the region in which the $k-$th approximator is active, i.e. each approximator is active in it's own region of support,

$$S_k = \{\alpha \in \mathcal{D}_\alpha |\ \|\alpha - c_k\| < \mu\}$$

and $\mathcal{D}_\alpha$ is a compact region in which α is defined. Then the total region of function approximation is the union of all locally supported regions, $\mathcal{A}^{N(t)} = \cup_{1 \le k \le N(t)} S_k$. Finally,

$$\hat{C}_{DL}(\alpha) = \begin{cases} \sum \frac{\omega_k(\alpha)}{\sum_{k=1}^{N} \omega_k(\alpha)} & , \quad \alpha \in \mathcal{A}^{N(t)} \\ 0 & , \quad \alpha \in \mathcal{D}_\alpha - \mathcal{A}^{N(t)} \end{cases}$$

The next step is to establish a criteria to expand the approximation domain in $\mathcal{D}_\alpha$ as needed. Whenever α is outside of the supported region $\mathcal{A}^{N(t)}$, $\hat{C}_{DL} = 0$. So, the Dynamics of the system would be $\dot{\tilde{\mathbf{X}}} = \mathbf{A}_m \tilde{\mathbf{X}} + \mathcal{B} C_{DL}(\alpha)$. The Lyapunov function $V_0 = \tilde{X}^T(t) P \tilde{X}(t)$ will have a derivative

$$\dot{V}_0 = -\tilde{X}^T Q \tilde{X} + 2\tilde{X}^T P \mathcal{B}^T C_{DL}(\alpha).$$

If the magnitude of Drag/Lift function is small enough while the angle of attack for any wing section is outside it's supported area, i.e. $|C_{DL}(\alpha)| < \epsilon$, we can conclude that $\dot{V}_0 \le 0$ and the stability is guaranteed. If V_0 increases while $\tilde{X}^T Q \tilde{X} > 2\tilde{X}^T P \mathcal{B}^T \epsilon$, then $\|C_{DL}(\alpha)| > \epsilon$ and the algorithem needs to expand the approximation region. The following criteria is employed for structure adaptation using the above discussion:

- If α is inside the approximation region i.e. $\alpha \in \mathcal{A}^{N(t)}$, do nothing.
- Otherwise, if $\dot{V}_0$ while $\tilde{X}^T Q \tilde{X} > 2\tilde{X}^T P \mathcal{B}^T \epsilon$, check if there is at least one operating point which is not activated by an approximator. If "Yes" add a new center to those functions; else, do nothing.

Finally, using the projection operator [40] the update law would be

$$\dot{\hat{\boldsymbol{W}}} = \begin{cases} Proj(\hat{\boldsymbol{W}}, -\boldsymbol{\Phi} \mathcal{B}^T \boldsymbol{P} \tilde{\mathbf{X}}) & , \quad \alpha \in \mathcal{A}^{N(t)} \\ 0 & , \quad \text{otherwise} \end{cases}$$

In order to test the controller efficiency and tracking performance, we have employed the introdueced adaptive controller on a simplified 4DOF wing section. Figure 4 depicts the tracking performance, the simulated and approximated aerodynamic contribution to the equation of motion $\mathbf{n}_a(\mathbf{X}(t))$ and $\hat{\mathbf{n}}_a(\mathbf{X}(t))$, and number of local approximators for each wing section. Square and sinusoidal desired trajectories are applied for the second wing section allowing the other sections to be fixed. The number of local approximator is greater for square wave due to relative calculation complexity of steep edges of the wave form. The approximation performance of both desired trajectories are improving which confirms that the approximation works well reducing the error between real and approximated functions. The tracking performance is better for the square wave comparing to sinusoidal wave which is due to higher frequency contents of the square wave which leads to persistantly exciting identification signals.

Downloaded by UNIV OF CALIFORNIA LOS ANGELES on May 2, 2014 | http://arc.aiaa.org | DOI: 10.2514/6.2014-0086

Downloaded by UNIV OF CALIFORNIA LOS ANGELES on May 2, 2014 | http://arc.aiaa.org | DOI: 10.2514/6.2014-0086

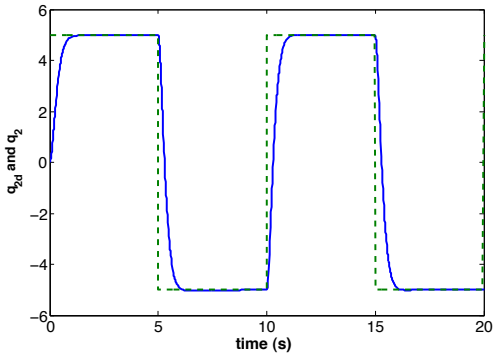

(a) Tracking performance for square wave

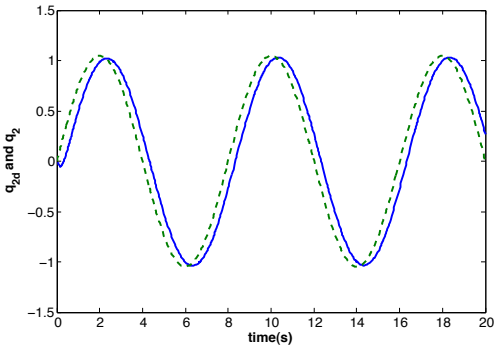

(b) Tracking performance for sinusoidal wave

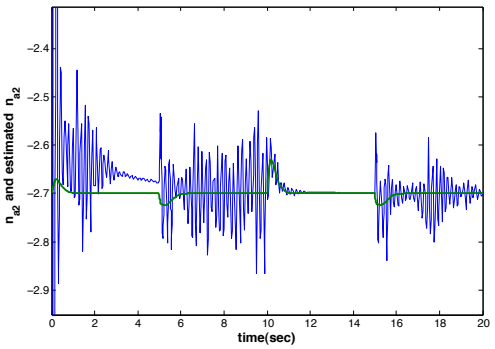

(c) Aerodynamic contribution and it's approximation

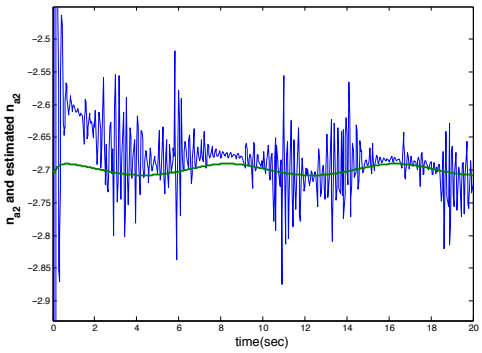

(d) Aerodynamic contribution and it's approximation

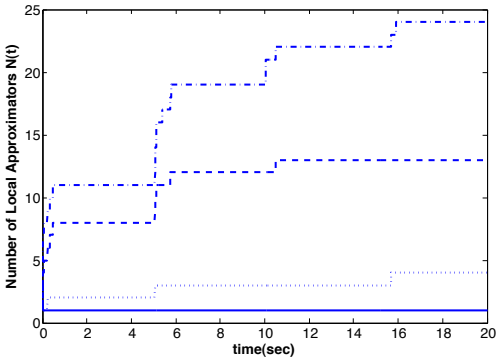

(e) Number of Local Approximators-Square wave

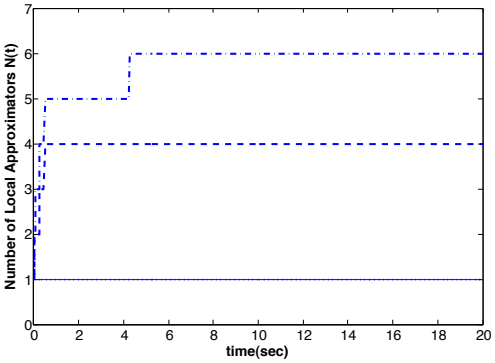

(f) Number of Local Approximators-Sinusoidal wave

Figure 4. The results for two different desiered trajectories, square wave on the left and sinusoidal wave on the right

VI. Numerical Results for Motion Identification

This section summarizes some of the initial solutions to the inverse kinematics and control problems described in the paper. The numerical experiments in this paper that study the identification of the motion of the bat for use in the closed loop control strategy are based on experimental data collected at Brown University. In [5, 26] Breuer and his colleagues describe a number of flight experiments with the specimen *Cynopterus brachyotis*. Figure 5 depicts the raw trajectories of three dimensional feature points on the bat in flight.

The location of the joints associated with the shoulder (b), elbow (c) and wrist (d) are depicted. Figure 6-a depicts two separate frames, number 1 and 110, in the data set under study. The body fixed frames having basis $\boldsymbol{b}_1, \boldsymbol{b}_2, \boldsymbol{b}_3$ are depicted. A number of points not used in the identification procedure that are located on wing membranes are shown in red. The ability of the DH kinematic model to represent accurately the experimental motion depends in part on the magnitude of flexibility effects. To gain some measure of the size of flexibility effects, the variation of the lengths between points fixed on the body of the bat are plotted in Figures 6-b and 6-c. In Figure 6-b, the distances between points located on the hip and sternum, sternum and shoulder, hip, and shoulder, are plotted versus the sample data point number. If the points were located on a rigid body, these points would plot as constant and would not deviate from the average.

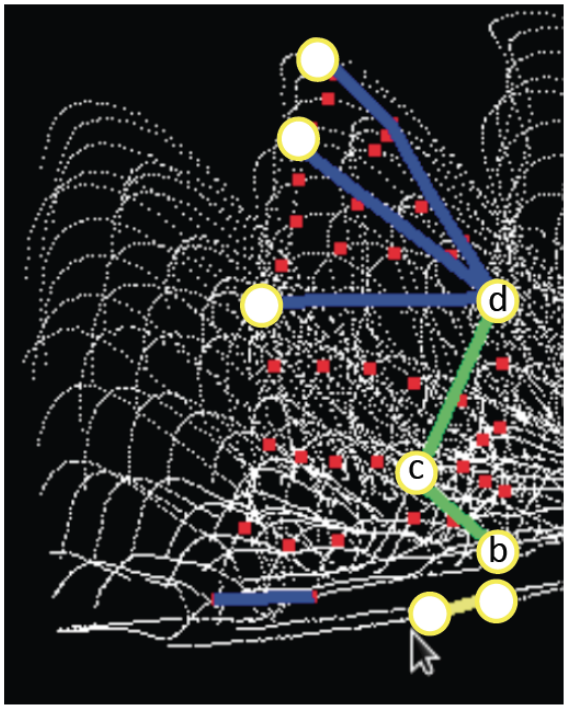

Figure 5. SCHEMATIC OF RAW DATA AND DH MODEL POINTS AT SHOULDER (B), ELBOW (C), WRIST(D) data provided by Dr. Breuer, Brown University

Figure 6-c depicts the deviation from the average shown in Figure 6-b in comparison to the tip motion of digit 3. The error or departure from the assumption of rigid motion on the body is less than 1% for much of the motion. Figures 6-d and 6-e depict the identified base body motion for the bat flight. The reconstructed motion of the bat body is compared in Figure 6-f to the raw data. We see that the identification procedure is able to reproduce the observed motion, providing confidence in the assumption that a rigid body motion is justified.

Downloaded by UNIV OF CALIFORNIA LOS ANGELES on May 2, 2014 | http://arc.aiaa.org | DOI: 10.2514/6.2014-0086

Downloaded by UNIV OF CALIFORNIA LOS ANGELES on May 2, 2014 | http://arc.aiaa.org | DOI: 10.2514/6.2014-0086

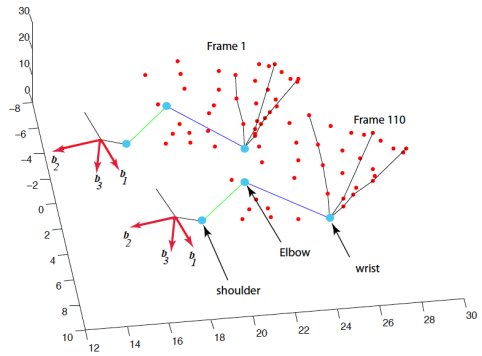

(a) Raw 3D Feature Points, Frames 1 and 110

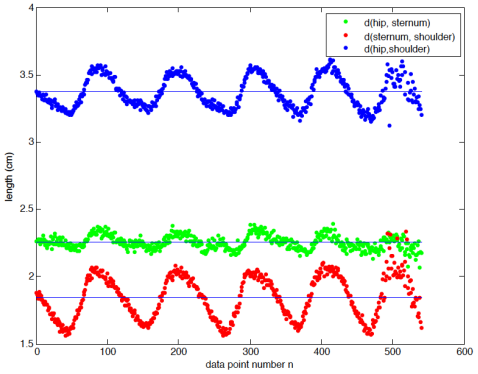

(b) Relative Motion of Points on Base Body

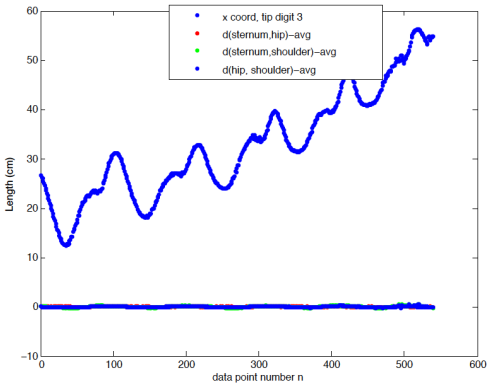

(c) Comparison of Digit 3 Tip Motion and Deviation from Rigid Body Motion

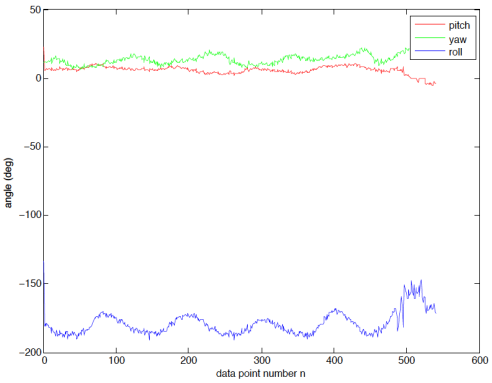

(d) Identification of Base Body Motion, Yaw-Pitch-Roll Angles

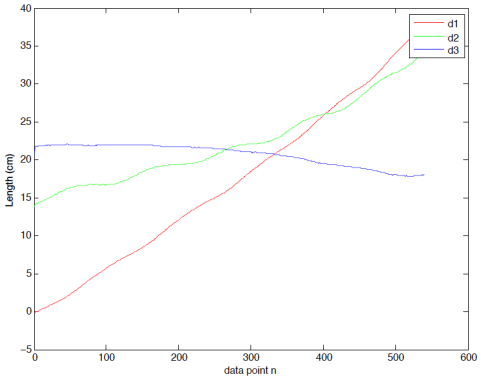

(e) Identification of Base Body Motion, Yaw-Pitch-Roll Angles

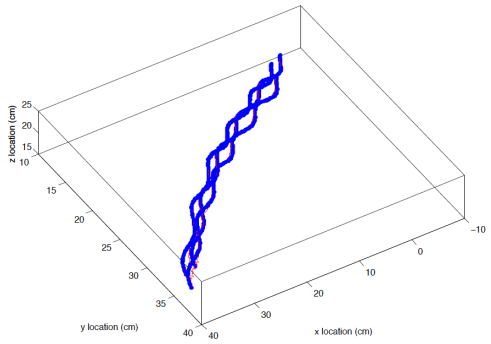

(f) Comparison of Raw and Identified Base Body Motion

Figure 6. The results for Identification of Bat Flight Motion

VII. Conclusion

The LWL algorithem has been employed to adaptively expand the approximation domain of drag and lift profiles. The results show that the algorithem effectively approximates the unknown aerodynamic contribution to the equations of motion of a robotic wing. The controller structure leads to a time responce with an effective transient performance in addition to an acceptable steady state responce. The identification of body and wing motion of the bat justified the assumption of rigid body and the identified trajectiries help reconstruct the wing and body motion.

VIII. Acknowledgment

We would like to acknowledge research contributions made by Dr. Breuer and Dr. Swartz. Their research group provided 3D motion capture data and the kinematic model of a bat wing. The adaptive flight controller which is derived in this paper was based on the base body trajectories and wing motions identified from their data.

Downloaded by UNIV OF CALIFORNIA LOS ANGELES on May 2, 2014 | http://arc.aiaa.org | DOI: 10.2514/6.2014-0086

References

[1]I.P. Murphy, S.Dadashi, J.Gregory, Y.Lei, J.Bayandor, A.J.Kurdila, "Modeling and Adaptive Control for Tracking Wing Trajectories," *IMECE 2013 Conference*, San Diego, CA, Nov 2013

[2]Bahlman, J.W., Swartz, S.M., and Breuer, K.S. "Design and Charaterization of a Multi-Articulated Robotic Bat Wing", *Bioinspiration & Biomimetics*, Vol. 8, 016009, 2013.

[3]J. Bayandor, G. Bledt, S. Dadashi, A. Kurdila, I. Murphy, and Y. Lei, "Adaptive Control for Bioinspired Flapping wing Robots," *Proceedings of the 2013 American Control Conference*, Washington, DC, June 17-19, 2013.

[4]C. Berg and J. Rayner, "The Moment of Inertia of Bird Wings and the Inertial Power Requirement for Flapping Flight," *J. Exp. Biol.*, Vol. 198, pp.1655-64, 1995.

[5]A.J. Bergou, S.M. Swartz, K.S. Breuer, and G. Taubin, "3D Reconstruction of Bat Flight Kinematics from Sparse Multiple Views," *proceedings of the IEEE ICCV: Int. Conf. on Computer Vision and Workshop on Dynamic Shape Capture*, 2011.

[6]G. Bradski, A. Barrientos, C. Rossi, and K. Breuer, "Biomechanics of Smart Wings in a Bat Robot: Morphing Wings using SMA Actuators," *Bioinspir. Biomim.*, Vol. 7, 036006, 2012.

[7]A. Hedenstrom, L.C. Johansson, M. Wolf, R. von Busse, Y. Winter, and G.R. Spedding, "Bat Flight Generates Complex Aerodynamic Tracks," *Science*, Vol. 316, pp. 894-897, 2007.

[8]A. Hedenstrom, F. Muijres, R. von Busse, L.C. Johansson, Y. Winter, and G.R. Spedding, "High Speed Stereo DPIV Measurement of Wakes of Two Bat Species Flying Freely in a Wind Tunnel," *Exp. Fluids*, Vol. 46, pp. 923-932, 2009.

[9]T.Y. Hubel, N.I. Hristov, S.M. Swartz, and K.S. Breuer, "Changes in Kinematics and Aerodynamics Over a Range of Speeds in *Tadarida brasiliensis*, the Brazilian Free-Tailed Bat," *J.R. Soc. Interface*, Vol. 9, pp. 1120-1130, 2012.

[10]T.Y. Hubel, D.K. Swartz, and K.S. Breuer, "Wake Structure and Wing Kinematics: The Flight of the Lesser Dog-Faced Fruit Bat, *Cynopterus brachyotis*, *J. Exp. Biol.*, Vol. 213, pp. 3427-3440, 2010.

[11]J. Iriarte-Diaz, "Flight Performance in Bats and Its Ecomorphological Implications," *PhD Thesis*, Department of Ecology and Evolutionary Biology, Brown University, Providence, Rhode Island, 2009.

[12]J. Irarte-Diaz, D.K. Riskin, D.J. Willis, K.S. Breuer, and S.M. Swartz, "Whole-Body Kinematics of a Fruit Bat Reveal the Influence of Wing Inertia on Body Accelerations," *J. Exp. Biol.*, Vol. 214, pp. 1546-1553, 2011.

[13]J. Iriarte-Diaz and S.M. Swartz, "Kinematics of Slow Turn Maneuvering in the Fruit Bat *Cynopterus Brachyotis*," *J. Exp. Biol*, Vol. 211, pp. 3478-3489, 2008.

[14]G. Koekkoek, F.T. Muijres, L.C. Johansson, M. Stuiver, B.W. van Oudheusden, and A. Hedenstrom, "Stroke Plane Angle Controls Leading Edge Vortex in a Bat-Inspired Flapper," *C.R. Mec.*, Vol. 340, pp. 95-106, 2012.

[15]A. J. Kurdila, A. Leonessa, and J. Vignola, *Dynamics and Control of Robotic Systems*, accepted for publication, Birkhauser, 2013.

[16]L.C. MacAyeal, D.K. Riskin, S.M. Swartz, and K.S. Breuer, "Climbing Flight Performance and Load Carrying in Lesser Dog-Faced Fruit Bats (Cynopterus brachyotis)," *J.Exp. Biol.*, Vol. 214, pp. 786-793, 2011.

[17]F. T. Muijres, G. Spedding, Y. Winter, and A. Hedenstrom, "Actuator Disk Model and Span Efficiency of Flapping Flight in Bats Based on Time-Resolved PIV Measurements," *Exp. Fluids*, Vol. 51, pp. 511-525, 2011.

[18]F.T. Muijres, M.S. Bowlin, L.C. Johansson, and A. Hedenstrom, "Vortex Wake, Downwash Distribution, Aerodynamic Performance and Wingbeat Kinematics in Slow-Flying Pied Flycatchers," *J.R. Soc. Interface*, Vol. 9, pp. 292-303, 2012.

[19]F.T. Muijres, L.C. Johansson, R. Barfield, M. Wolf, G.R. Spedding, and A. Hedenstrom, "Leading-Edge Vortex Improves Lift in Slow-Flying Bats," *Science*, Vol. 319, pp. 1250-1253, 2008.

[20]U.M. Norberg, "Functional Osteology and Myology of the Wing of the Dog-Faced Bat; *Rousettus aegyptiacus*," *Zoomorphology*, Vol. 73, pp. 1-44, 1972.

[21]U.M. Norbert, "Aerodynamics, Kinematics, and Energetics of Horizontal Flapping Flight in the Long-Eared Bat *Plecotus auritus*," *J. Exp. Biol.*, Vol. 65, pp. 179-212, 1976.

[22]U.M. Norberg, T.H. Kunz, J. F. Steffenson, Y. Winter, and O. von Helverson, "The Cost of Hovering and Forward Flight in a Nectar-Feeding Bat, *Glossophaga soricina*, Estimated from Aerodynamic Theory," *J. Exp. Biol.*, Vol. 182, pp. 207-227, 1993.

[23]U.M. Norberg and J.M.V. Rayner, "Ecological Morphology and Flight in Bats (Mammalia; Chiroptera): Wing Adaptations, Flight Performance, Foraging Strategy and Echolocation," *Phil. Trans. R. Soc. B*, Vol. 316, pp. 335-427, 1987.

[24]M.F. Platzer, K.D. Jones, J. Young, and C.S. Lai, "Flapping-Wing Aerodynamics: Progress and Chalnges," *AIAA Journal*, Vol. 46, No. 9, pp. 2136-2149, September, 2008.

[25]D.K. Riskin, J.W. Bahlman, T.Y. Hubel, J.M. Ratcliffe, T.H. Kunz, and S.M. Swartz, "Bats Go Head-Under-Heels: the Biomechanics of Landing on a Celing," *J. Exp. Biol.*, Vol. 212, pp. 945-953, 2009.

[26]D.K. Riskin, D.J. Willis, J. Iriarte-Diaz, T.L. Hedrick, M. Kostandov, J. Chen, D. H. Laidlaw, K. S. Breuer, and S. Swartz, "Quantifying Complexity of Bat Wing Kinematics," *Journal of Theoretical Biology*, Vol. 254, pp. 604-615, 2008.

[27]S.P. Sane and M.H. Dickinson, "The Control of Flight Force by a Flapping Wing: Lift and Drag Production," *J. Exp. Biol.*, Vol. 204, pp. 2607-2626, 2004.

[28]A. Song, X. Tian, E. Israeli, R. Galvao, K.L. Bishop, S.M. Swartz, and K. Breuer, "Aeromechanics of Membrane Wings with Implications for Animal Flight," *AIAA J.*, Vol. 46, pp. 2096-2106, 2008.

[29]M.W. Spong, S. Hutchinson, and M. Vidyasagar, *Robot Modeling and Control*, John Wiley & Sons, 2006.

[30]S.M. Swartz, M. S. Groves, H.D. Kim, and W.R. Walsh, "Mechanical Properties of Bat Wing Membrane Skin," *J. Zool.*, Vol. 239, pp. 357-378, 1996.

[31]S.M. Swartz and K.M. Middleton, "Biomechanics of the Bat Limb Skeleton: Scaling, Material Properties and Mechanics," *Cells Tissues Organs*, Vol. 187, pp. 59-84, 2008.

[32]B. Siciliano, L. Sciavicco, L. Villani, and G. Oriolo, *Robotics Modelling, Planning and Control*, Springer-Verlag, 2010.

[33]H.E. Taha, M.R. Hajj, and A.H. Nayfeh, "Flight Dynamics and Control of Flapping-Wing MAVs: A Review," *Nonlinear Dynamics*, Vol. 70, pp. 907-939, 2012.

[34]M. Thollesson and U.M. Norberg, "Moments of Inertia of Bat Wings and Body," *J. Exp. Biol.*, Vol. 158, pp. 19-35, 1991.

[35]X. Tian, J. Iriarte-Diaz, K. Middleton, R. Galvao, E. Israeli, A. Roemer, A. Sullivan, A. Song, S.M. Swartz, and K. Breuer, "Direct Measurements of the Kinematics and Dynamics of Bat Flight," *Bioinspir. Biomim.*, Vol. 1, S10-8.

[36]B.W. Tobalske, T.L. Hedrick, K.P. Dial, and A. Biewener, "Comparative Power Curves in Bird Flight," *Nature*, Vol. 421, pp. 363-366, 2003.

[37]P. Watts, E.J. Mitchell, and S.M. Swartz, "A Computation Model for Estimating the Mechanics of Horizontal Flapping Flight in Bats," *J. Exp. Biol.*, Vol. 204, pp. 2873-2898, 2001.

[38]M. Wolf, L.C. Johansson, R. von Busse, Y. Winter, and A. Hedenstrom, "Kinematics of Flight and the Relationship to the Vortex Wake of a Pallas' Long Tongued Bat (*Glossophaga soricina*)," *J. Exp. Biol.*, Vol. 213, pp. 2142-2153, 2010.

[39]Yiming Chenn, Jay A. Farrel "Self-Organizing Approximation Based Control with L1 Transient Performance Guarantees " *American Control Conference*, pp. 1169-1175, 2011.

[40]M. Krstic, I. Kanellakopoulos, and P. Kokotovic, "Nonlinear and Adaptive Control Design" *Willey*, 1995.

Downloaded by UNIV OF CALIFORNIA LOS ANGELES on May 2, 2014 | http://arc.aiaa.org | DOI: 10.2514/6.2014-0086